# LA-UR-17-20914



Title: Nanoindentation of Electropolished FeCrAl Alloy Welds

Author(s): Weaver, Jordan
Aydogan, Eda
Mara, Nathan Allan
Maloy, Stuart Andrew

Intended for: Report

Issued: 2017-02-13 (rev.1)

# *Nanoindentation of Electropolished FeCrAl Alloy Welds*

*Prepared for*
*U.S. Department of Energy*
*xxxxx Campaign*

*Jordan S. Weaver*
*Eda Aydogan*
*Nathan A. Mara*
*Stuart A. Maloy*

*February 8, 2017*

**FCRD-FUEL-2017-000xxx**

# SUMMARY

The present report summarizes Berkovich nanoindentation modulus and hardness measurements on two candidate FeCrAl alloys (C35M and C37M) on as-received (AR) and welded samples. In addition, spherical nanoindentation stress-strain measurements were performed on individual grains to provide further information and demonstrate the applicability of these protocols to mechanically characterizing welds in FeCrAl alloys. The indentation results are compared against the reported tensile properties for these alloys to provide relationships between nanoindentation and tensile tests and insight into weld-softening for these FeCrAl alloys.

Hardness measurements revealed weld-softening for both alloys in good agreement with tensile test results. C35M showed a larger reduction in hardness at the weld center from the AR material compared to C37M; this is also consistent with tensile tests. In general, nanohardness was shown to be a good predictor of tensile yield strength and ultimate tensile stress for FeCrAl alloys. Spherical nanoindentation measurements revealed that the fusion zone (FZ) + heat affected zone (HAZ) has a very low defect density typical of well-annealed metals as indicated by the frequent pop-in events. Spherical nanoindentation yield strength, Berkovich hardness, and tensile yield strength measurements on the welded material all show that the C37M welded material has a higher strength than C35M welded material. From the comparison of nanoindentation and tensile tests, EBSD microstructure analysis, and information on the processing history, it can be deduced that the primary driver for weld-softening is a change in the defect structure at the grain-scale between the AR and welded material. These measurements serve as baseline data for utilizing nanoindentation for studying the effects of radiation damage on these alloys.

# TABLE OF CONTENTS

SUMMARY .......... iv

1. Introduction .......... 1

2. Materials and Methods .......... 1

3. Results .......... 4
   - 3.1 Berkovich Nanoindentation .......... 4
   - 3.2 Spherical Nanoindentation .......... 8

4. Discussion .......... 11
   - 4.1 Weld-softening .......... 11
   - 4.2 Spherical nanoindentation across gradient microstructures .......... 11

5. Conclusions .......... 12

6. Future Work .......... 13

7. References .......... 13

# FIGURES

Figure 1. Representative EBSD micrographs of the AR C35M and C37M samples taken from Ref. [5]. The inverse pole figure (IPF) maps, image quality (IQ) maps, and grain reference orientation distributions (GROD) are shown. .......... 2

Figure 2. (a) Sample schematic of FeCrAl weld samples, (b) EBSD inverse pole figure (IPF) map of C35M alloy, and (c) EBSD IPF map of C37M alloy. The approximated weld centers are drawn as dotted white lines. The grayscale bars above each map roughly show where the fusion zone (FZ) ends and the heat-affected zone begins (HAZ). .......... 3

Figure 3. Cumulative grain diameter distributions for C35M and C37M alloys in the FZ and HAZ. Grain diameter analysis comes from EBSD micrographs. .......... 3

Figure 4. Load-displacement, modulus, and hardness measurements for (a-c) C35M, (d-f) C37M, and (g-i) fused silica, respectively. For each test, the average modulus and hardness was measured for the specified displacement range. The average and standard deviations listed are based on the total number of tests. .......... 5

Figure 5. Nanoindentation hardness (a, b) and modulus (c, d) measurements for welded samples. The solid and dotted lines represent the average and ± one standard deviation for the AR samples. .......... 6

Figure 6. Comparison of hardness and tensile yield stress and ultimate tensile stress (UTS) measurements. Note that the yield stress is an engineering stress and the UTS is a true stress value. No error bars were available for the welded material. The large error bar for C37M AR is due to the large variance in the tensile data. .......... 7

Figure 7. (a) Representative load-displacement curves for the 8 and 100 micron radius indenters showing pop-ins (b) Representative indentation stress-strain curves for the 8 and 100 micron radius indenters showing the pop-in indentation stress. (c) Cumulative indentation pop-in stress distributions for both indenter sizes. The totals come from all test data across both alloys and zones (FZ and HAZ) in the welds. Note that roughly 50% of the 100 micron radius tests showed pop-ins while 100% of the 8 micron radius tests showed pop-ins. .......... 8

Figure 8. (a) Representative load-displacement curves for 8 micron radius tests for C35M and C37M alloys in the FZ and HAZ, (b) corresponding grain orientations represented in the inverse pole figure, (c-d) indentation stress-strain curves, and (e-f) locations of tests on the weld microstructures (grayscale EBSD-IPF maps). .......... 9

Figure 9. (a) Representative load-displacement curves for 100 micron radius tests for C35M and C37M alloys in the FZ and HAZ, (b) corresponding grain orientations represented in the inverse pole figure, (c-d) indentation stress-strain curves, and (e-f) locations of tests on the weld microstructures (grayscale EBSD-IPF maps). .......... 10

Figure 10. Weld microstructure (modified from [5]) showing the FZ, HAZ, and BM. Listed below are the expected mechanical responses from different indenter sizes ranging from single grains/crystals to polycrystalline/bulk-like volumes. Note that only 10 (single grain) and 100 micron (single grain at the edge grain boundary effects) radius indenter measurements were made in the FZ and HAZ in this report. .......... 12

Figure 11. Comparison of indentation measurements from pyramidal and spherical tip protocols. (a) Representative Berkovich hardness versus indentation depth in the FZ for C35M and C37M alloys (see Table 1 for quantitative results). (b) Representative indentation stress-strain curves for spherical tips in the FZ for C35M and C37M (see Table 2 for quantitative results). Note all tests shown are inside individual grains. .......... 13

# TABLES

Table 1. Average modulus, hardness, and weld-softening values for C35M and C37M FeCrAl alloys. The error represents ± one standard deviation. .......... 6

Table 2. Average indentation modulus, strength, and work-hardening values for C35M and C37M FeCrAl alloys in the FZ and HAZ. The error represents ± one standard deviation. .......... 10

Intentionally Blank

# 1. Introduction

FeCrAl alloys are being explored for accident tolerant fuel cladding material because of their excellent properties: high temperature oxidation resistance, aqueous corrosion resistance, low radiation-induced swelling, and tolerance to loss-of-coolant accident conditions [1-4]. The successful development and application of these alloys requires substantial mechanical and structural characterization efforts and radiation experiments. Furthermore, the evaluation of the weldability of these alloys and the structure-property relationships of welded material are critical. Current efforts at Oak Ridge National Laboratory (ORNL) under the Department of Energy's (DOE) Nuclear Engineering Enabling Technologies (NEET) program focused on developing modern, nuclear grade FeCrAl alloys are primarily using tensile testing to evaluate the mechanical properties [2, 5, 6]. Weld mechanical properties are isolated from the base material (BM) using digital image correlation (DIC) strain measurements on tensile bars which contain welded and BM [3, 6]. In this report, as-received (AR) is used to designate samples that were not welded and BM is used to designate material on welded samples that is unaffected by the weld. Microscale (grain-scale) mechanical testing as opposed to bulk-mechanical testing has the potential to offer complimentary and new insights into the mechanical behavior of these alloys in the unirradiated/non-welded, welded, and irradiated/welded conditions. Nanoindentation in particular has proven highly valuable at quantifying the mechanical behavior of welds and ion irradiated materials with little effort required to prepare samples and conduct a large number of tests (e.g., [7-9]). However, the analysis, interpretation, and relation of results to uniaxial mechanical properties can be time consuming and fraught with uncertainty. Some of this uncertainty can be eliminated by using improved indentation protocols. Recent advances in spherical nanoindentation protocols [10] have shown that reliable grain-scale indentation stress-strain curves (the initial elastic, yield, and work-hardening response) can be measured on ion irradiated steel [11], and the indentation stress-strain response can be converted to a uniaxial stress-strain response to provide more meaningful estimates of uniaxial strength [12, 13]. In this report, nanohardness and spherical nanoindentation stress-strain measurements will be employed to characterize the grain scale response of two candidate FeCrAl alloys on welded and AR material and compared with ORNL bulk-tensile results.

# 2. Materials and Methods

Two of the seven candidate FeCrAl alloys under development by ORNL were provided for nanoindentation testing designated as C35M and C37M. The base alloy, C35M, is completely ferritic with 13Cr-5Al-2Mo in weight percentage; the alloy C37M is the same with an additional 2 wt.% Al [5]. A small addition of Al was added to explore the regions of α' embrittlement and weld cracking in the design space of nuclear grade FeCrAl alloys [5]. Autogenous, bead-on-plate welding under an argon cover gas was used to produce crack free welded samples [5]. AR and welded samples were mechanically ground and polished followed by electropolishing prior to nanoindentation.

The microstructure and tensile properties of AR and welded C35M and C37M samples were characterized by ORNL [5, 6]. Electron backscatter diffraction (EBSD) micrographs from Ref. [5] of the AR material are shown in Figure 1. There is a clear difference between the two alloys in the amount of un-recrystallized (deformed) material. The un-recrystallized material contains small, elongated grains with significant in-grain misorientation which has higher defect densities than the recrystallized, defect free material. C35M has considerably more remaining un-recrystallized (deformed) material. Estimates are that C37M is >90% recrystallized while C35M experienced only moderate recrystallization [5]. This is despite the materials having been processed in the same manner. The average tensile yield strengths of the AR material for C35M and C37M are 627.4 ± 13.8 MPa and 587.2 ± 33 MPa [6]. There was no significant difference in the ultimate tensile strength (UTS) with the averages falling between 717 and 721 MPa [6]. Tensile data was taken from

Ref. [6] with the exception of C35M welded material which was taken from Ref. [5]. This was done to compile data with error estimates for the same test geometry where available.

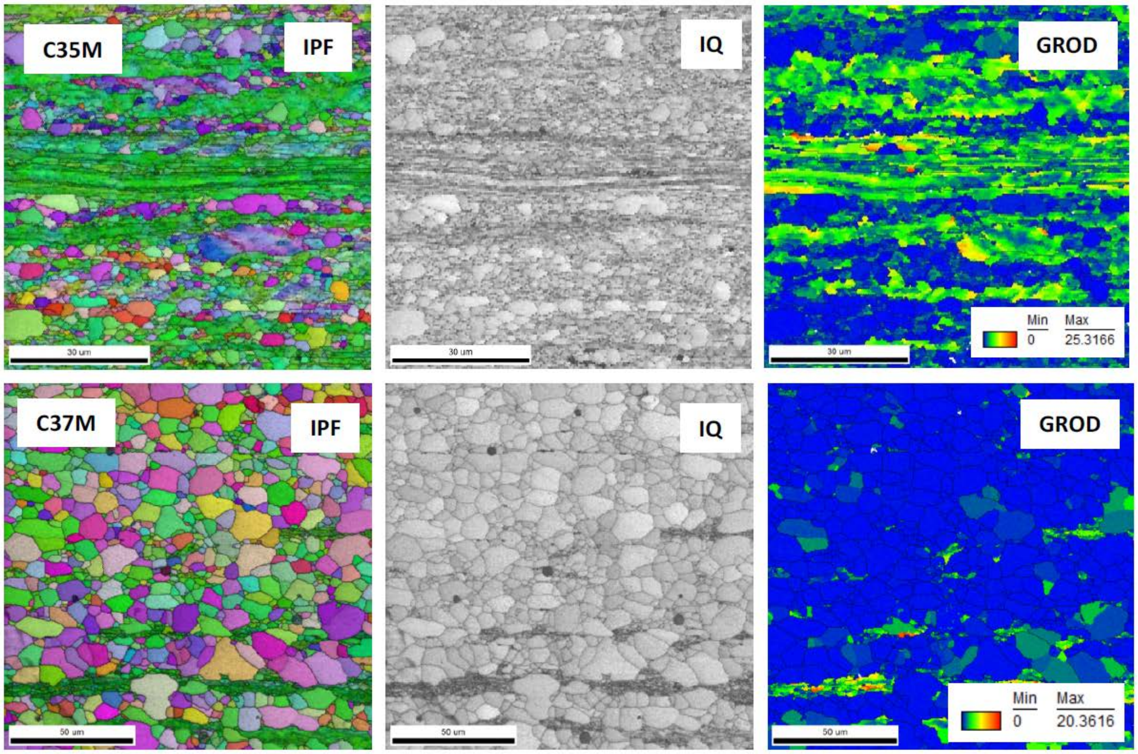


**Figure 1. Representative EBSD micrographs of the AR C35M and C37M samples taken from Ref. [5]. The inverse pole figure (IPF) maps, image quality (IQ) maps, and grain reference orientation distributions (GROD) are shown.**

The fusion zone (FZ) and heat-affected zone (HAZ) show an increased grain size over the AR material. Figure 2 shows the microstructures of the welded samples in the FZ and HAZ. Even between the FZ and HAZ, there is a significant change in grain size, with the FZ having the largest grains. Figure 3 shows the difference in the cumulative grain diameter distributions in the FZ compared to the HAZ for both alloys determined from EBSD data in Figure 2. Weld-softening, a reduction in tensile yield strength for the welded material, was observed for both alloys: 18% for C35M and 12% for C37M [5]. The AR and welded samples showed ductile fracture surfaces with the exception of C37M welded samples which showed cleavage fracture surfaces for every test [5]. It is not clear why the C37M weld exhibited more brittle fracture. The weld-softening is likely a combination of an increase in grain size and eliminated deformation (defects) which both reduce the tensile yield strength. This will be explored with grain-scale nanoindentation measurements which are unaffected by the grain size.

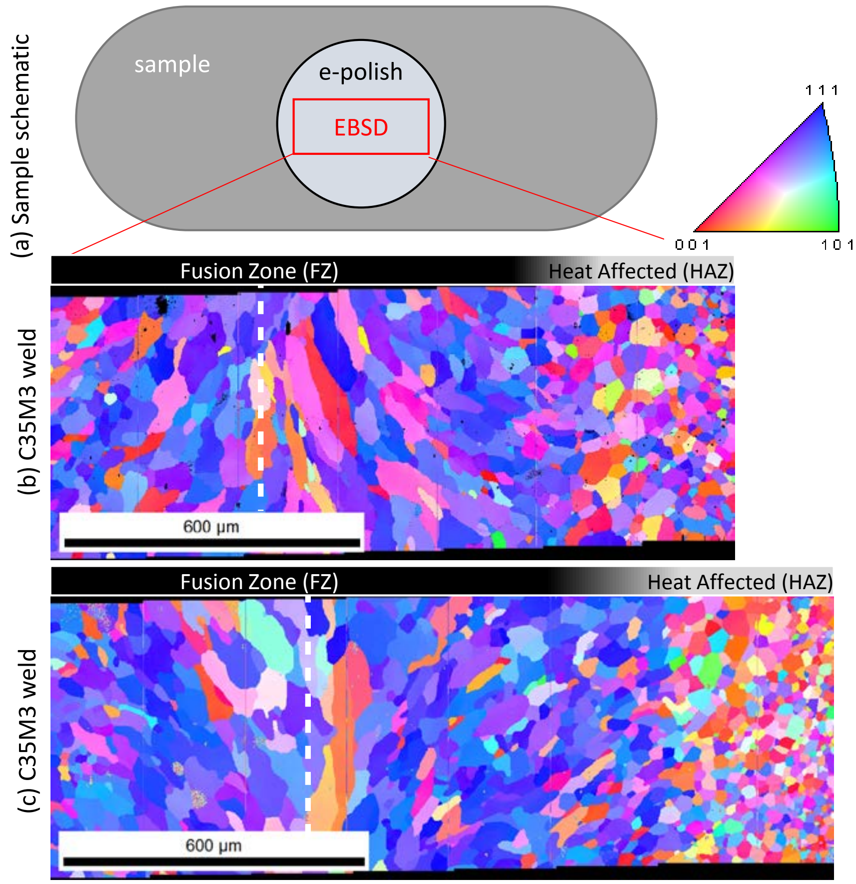


**Figure 2. (a) Sample schematic of FeCrAl weld samples, (b) EBSD inverse pole figure (IPF) map of C35M alloy, and (c) EBSD IPF map of C37M alloy. The approximated weld centers are drawn as dotted white lines. The grayscale bars above each map roughly show where the fusion zone (FZ) ends and the heat-affected zone begins (HAZ).**

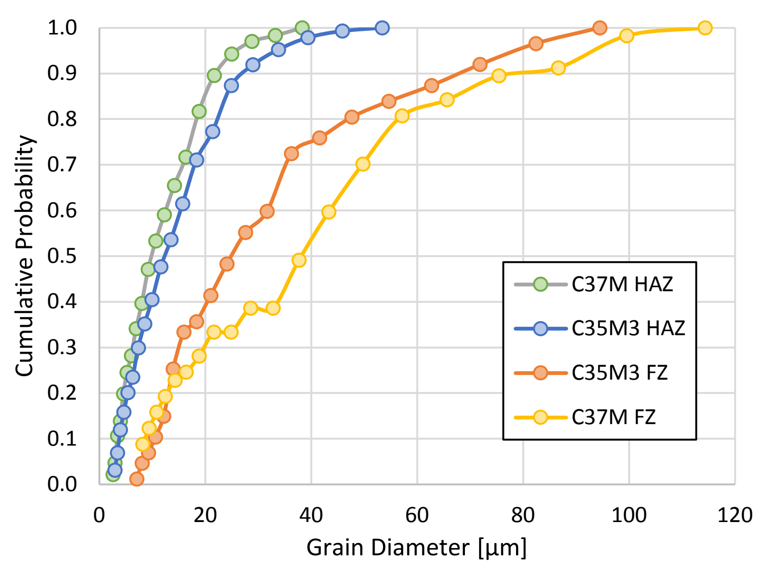


**Figure 3. Cumulative grain diameter distributions for C35M and C37M alloys in the FZ and HAZ. Grain diameter analysis comes from EBSD micrographs.**

Nanoindentation tests were performed on an MTS NanoXP Nano-Indenter with a constant strain rate (loading rate divided by the load) of 0.05 $s^{-1}$ and continuous stiffness measurement (CSM) of 45 Hz frequency and 2 nm displacement amplitude. The CSM allows for the contact stiffness to be measured throughout the test by oscillating the tip which subsequently generates many small unloads [14, 15]. For hardness and modulus measurements, indents were made with a diamond, pyramidal (Berkovich) tip to a final displacement of 500 nm on all FeCrAl samples. The Oliver-Pharr method [16] was used for modulus and hardness analysis. More specifically, a four term tip contact area function ($C_{0,1,2,3} = 25.2, 680, -2214, 994$) was determined from tests on a fused silica standard with an indenter Young's modulus and Poisson's ratio of 1130 GPa and 0.07 (diamond). This area function was used to analyze tests on FeCrAl samples along with a sample Poisson's ratio of 0.3. For determination of the indentation stress-strain behavior, conical-spherical, diamond tips with nominal radii of 8 μm and 100 μm were used to indent to depths of 400-800 and 500 nm, respectively. The load, displacement, and contact stiffness data were converted to indentation stress and strain using analysis protocols by Kalidindi and Pathak [10, 17].

EBSD was performed using an FEI XL30 scanning electron microscope (SEM) and TSL EDAX digiview detector with OIM Data Collection/Analysis software. Backscatter electron (BSE) images were taken on a FEI Inspect SEM. EBSD maps were used to approximately determine the weld center (dotted lines on Figure 2). BSE images were used to measure the distance of Berkovich indents from the weld center line. EBSD was also used to determine the grain orientations at spherical indentation sites and whether the indents were in the FZ or HAZ. The weld center, FZ, and HAZ were approximated based on the changes in grain morphology.

Spherical nanoindentation properties were determined as follows. The indentation modulus is the elastic response of the sample and is physically related to the crystal elastic constants for an elastically anisotropic material [18, 19]. The indentation modulus comes directly from the load-displacement data, indenter radius, and indenter elastic properties (diamond) according to Hertz's theory [10, 20, 21] as opposed to a linear regression of the elastic indentation stress-strain data. The indentation yield strength was determined as a 0.2% strain offset on the indentation stress-strain curve. The pop-in stress was determined as the average stress during the pop-in event before the stress drop occurs on the indentation stress-strain curve. In the case where small pop-ins occurred (the 100 μm radius indenter), the yield strength was determined by back-extrapolating the post pop-in data with a linear regression to the 0.2% strain offset line. The indentation work-hardening for the 100 μm radius indenter was determined from the post-yield or post pop-in data that fell between strain offsets of 1% and 2% as the slope of a linear regression.

# 3. Results

## 3.1 Berkovich Nanoindentation

Berkovich nanoindentation modulus and hardness measurements on the AR material for C35M and C37M alloys along with a fused silica standard are shown in Figure 4. Both FeCrAl alloys show an indentation size effect for hardness (increased hardness at decreasing indentation depth). This is generally believed to be caused by an increase in the number of geometrically necessary dislocations as a function of decreasing depth due to the increasing strain gradient under the indenter at very shallow depths [22-24]. The magnitude of the indentation size effect varies significantly from test to test. Possible reasons for this behavior are surface roughness, varying oxide layer thickness, and hitting grain boundaries/varying dislocation densities. The indentation size effect is very sensitive to surface irregulars [25]. The average modulus was taken over a displacement range of 50-500 nm where it remained fairly constant with depth, and the average hardness was determined from a displacement range of 400-500 nm to lessen the influence of the indentation size effect on the measured value. The modulus values from nanoindentation on both samples ranges from ~200 to 250 GPa. This is higher than the expected bulk value of 170-180

GPa measured by resonant ultrasound spectroscopy [26]. It is possible that the area function determined from fused silica is not accurate enough to make precise modulus measurements given that the pile-up/sink-in behavior of the material is likely different between FeCrAl and fused silica [16, 27]. The data on fused silica is reported here to confirm the accuracy of the calibrated area function for fused silica which produced an average modulus and hardness of 73.5 ± 0.8 GPa and 9.72 ± 0.20 GPa, respectively.

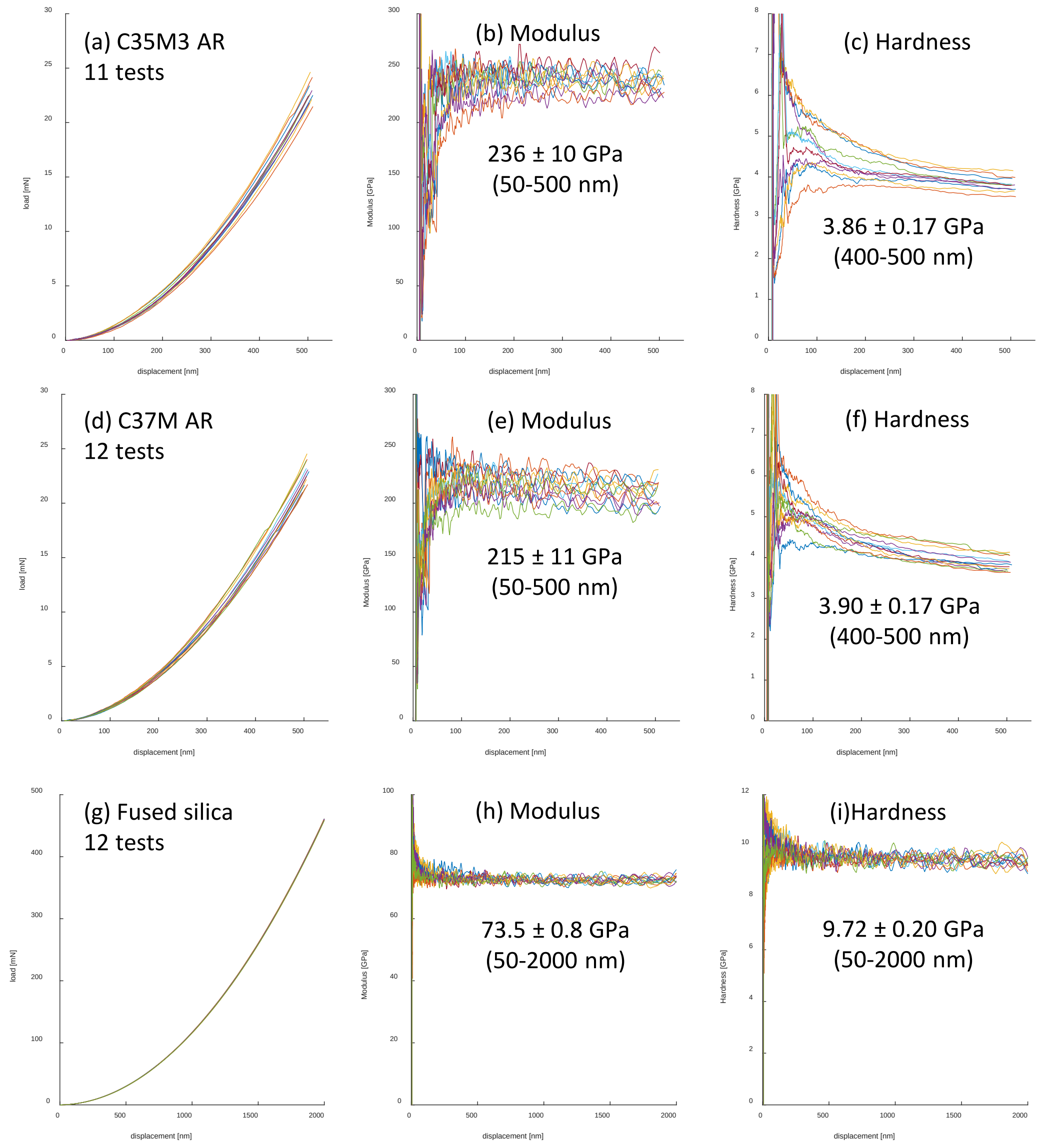


**Figure 4. Load-displacement, modulus, and hardness measurements for (a-c) C35M, (d-f) C37M, and (g-i) fused silica, respectively. For each test, the average modulus and hardness was measured for the specified displacement range. The average and standard deviations listed are based on the total number of tests.**

The modulus and hardness measurements on the weld samples are shown in Figure 5 as a function of their distance from the weld center. Each data point is a single test. These are compared against the average (solid line) and standard deviation (dotted lines) values for the AR material. For C35M, it is clear that the welded material is softer than the AR material, and there is a trend of increasing hardness moving away from the weld center. The hardness plateaus at a distance of ~ 500 microns which is also around where the FZ ends and the HAZ starts (see Figure 2). For C37M the welded material is also softer than the AR material, but to a lesser degree than C35M. In fact, the hardness quickly approaches the average value of the AR material away from the weld center line. The modulus of the welded and AR samples remained unchanged. There is a slight trend with decreasing modulus values approaching the weld center. It is possible that this is related to changes in chemical composition across the weld; however, since the data is within the variance of the AR material measurements, it is difficult to argue that the trend is significant. A summary of the modulus and hardness measurements on welded and AR samples is given in Table 1. In this case, the weld center is defined as material <100 microns from the weld center line. This was chosen as the definition since the hardness started to increase at distances >100 microns on both samples.

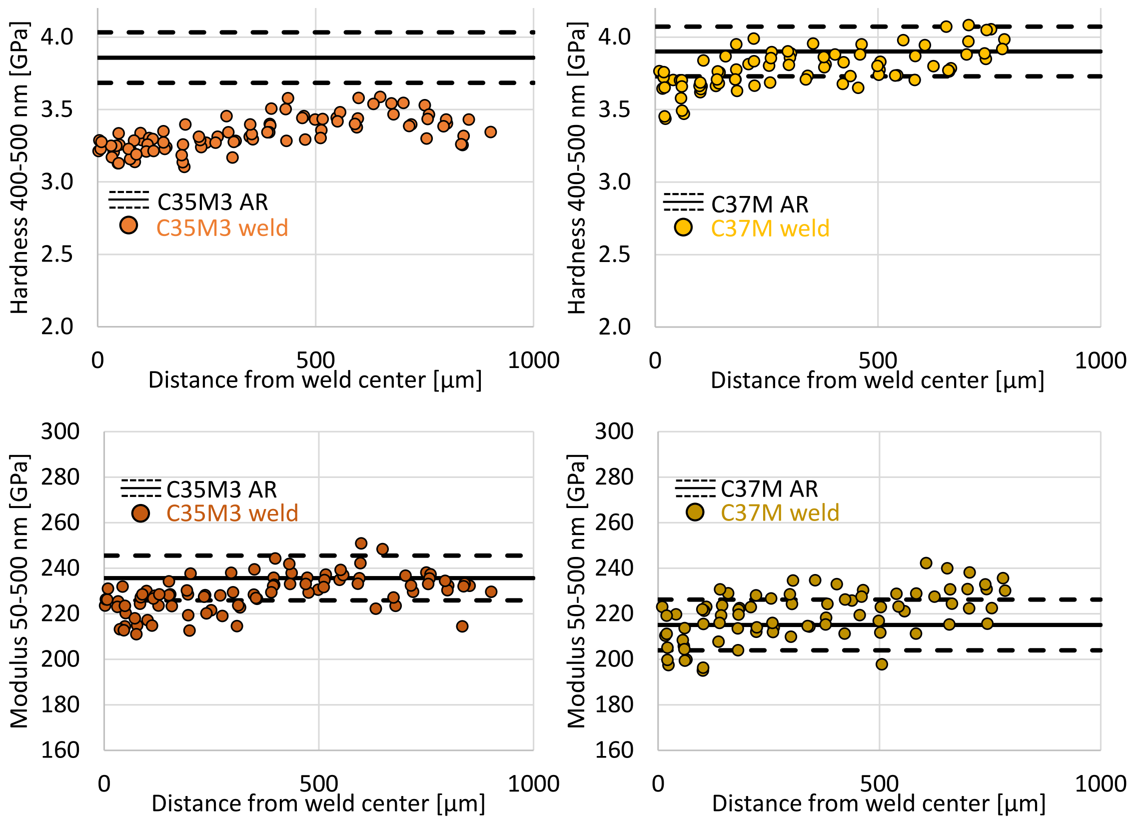


**Figure 5. Nanoindentation hardness (a, b) and modulus (c, d) measurements for welded samples. The solid and dotted lines represent the average and ± one standard deviation for the AR samples.**

**Table 1. Average modulus, hardness, and weld-softening values for C35M and C37M FeCrAl alloys. The error represents ± one standard deviation.**

| Sample | Modulus (50-500 nm) [GPa] | Hardness (400-500 nm) [GPa] | Weld-softening [%] | No. Tests |
|---|---|---|---|---|
| C35M AR | 236 ± 10 | 3.86 ± 0.17 | n/a | 11 |
| C35M weld center | 222 ± 6 | 3.23 ± 0.06 | 16 ± 4 | 19 |
| C37M AR | 215 ± 11 | 3.90 ± 0.17 | n/a | 12 |
| C37M weld center | 209 ± 8 | 3.63 ± 0.11 | 7 ± 5 | 15 |

Weld-softening, reduced hardness in the welded material compared to the AR material, occurs for both alloys. It is more severe for C35M (16 ± 4%) compared to C37M (7 ± 5%). This likely reflects the difference in the amounts of un-recrystallized/recrystallized grains between the two alloys in the AR material. The C35M alloy had considerably more un-recrystallized (deformed) grains (observed from EBSD micrographs, see Figure 1) than the C37M alloy. All the deformed grains have been removed in the FZ due to the melting process, and most of deformed grains have likely been removed from the HAZ due to the high temperatures creating largely defect free material in both regions.

A comparison of hardness measurements to uniaxial tensile straining measurements in Figure 6 shows that the hardness data captures similar trends seen in the tensile data. The weld-softening from hardness is approximately the same as the weld-softening from tensile tests. This is despite the large difference in length scale: mostly single grain measurements for nanoindentation and polycrystalline, bulk measurements for tensile specimens. The ratio of nanohardness to tensile yield strength and ultimate tensile stress are also given in Figure 6. The ratios of hardness to tensile yield stress are significantly higher than typical ratios (~3 for metals [28]). This could reflect a considerable amount of work-hardening under the indenter. In this case, a more appropriate ratio is the hardness of the true stress at a true strain of 8-20% [28]. For the AR material, the UTS or uniform elongation limit is ~10% true strain [5, 6]. For the welded material, the specimens reach the uniform elongation limit at a true strain of ~4.5% [5, 6]. The ratio of hardness to UTS given in Figure 6 is also higher than the expected relationship for metals (~3). However, it is much closer than the ratio of hardness to tensile yield strength. It may be that compression testing to higher true strains is required to determine the appropriate comparison between hardness and uniaxial tests for the theoretical ratio of ~3. Despite this, the current findings from this data show that hardness can be used to predict tensile stresses (yield and UTS) for FeCrAl alloys including FZ welded material using an average ratio of 6.5 for hardness/yield strength (engineering stress) and 5.1 for hardness/UTS (true stress). These values can range widely for other materials (e.g., stainless steels [29, 30]).

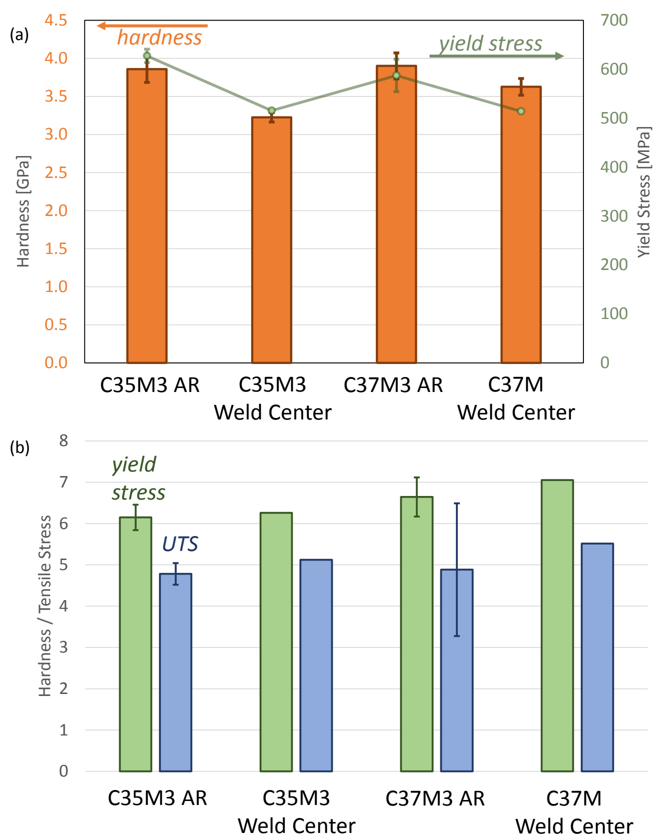


**Figure 6. Comparison of hardness and tensile yield stress and ultimate tensile stress (UTS) measurements. Note that the yield stress is an engineering stress and the UTS is a true stress value. No error bars were available for the welded material. The large error bar for C37M AR is due to the large variance in the tensile data.**

## 3.2 Spherical Nanoindentation

Spherical nanoindentation tests showed pop-ins (displacement or strain bursts) for both 8 and 100 µm radius indenters in the FZ and HAZ for both alloys. Representative load-displacement curves, indentations stress-strain curves, and the cumulative pop-in stress distributions for the two indenter sizes are shown in Figure 7. For both indenters, the indents were carefully placed inside individual grains rather than randomly placed as was done for the Berkovich indents. The average contact radius at the end of the tests for the 8 and 100 µm radius indenters was 1.2 ± 0.4 and 5.4 ± 0.3 microns, respectively. The large variance for the 8 µm indenter is partly due to the fact that half the tests were stopped at 400 nm and half were run to 800 nm depth. Regardless, it is clear that the primary indentation zone, defined as a cylinder under the indenter with radius equal to the contact radius and height of 2.4 times the contact radius [10, 31], is well within single grains in the FZ and HAZ.

The pop-in is believed to be a consequence of testing small volumes which do not contain a sufficient number of dislocation sources [32-34]. Large stresses are required to generate a source for plastic slip after which it becomes significantly easier for plastic deformation to continue [32-34]. The pop-in behavior shows a pronounced indenter size effect with decreasing pop-in load/stresses with increasing indenter sizes [33-36], which diminishes in deformed metals with higher dislocation densities [36-38]. The pop-in behavior on the FeCrAl welds is indicative of a well annealed metal which means the FZ and HAZ have relatively low defect densities.

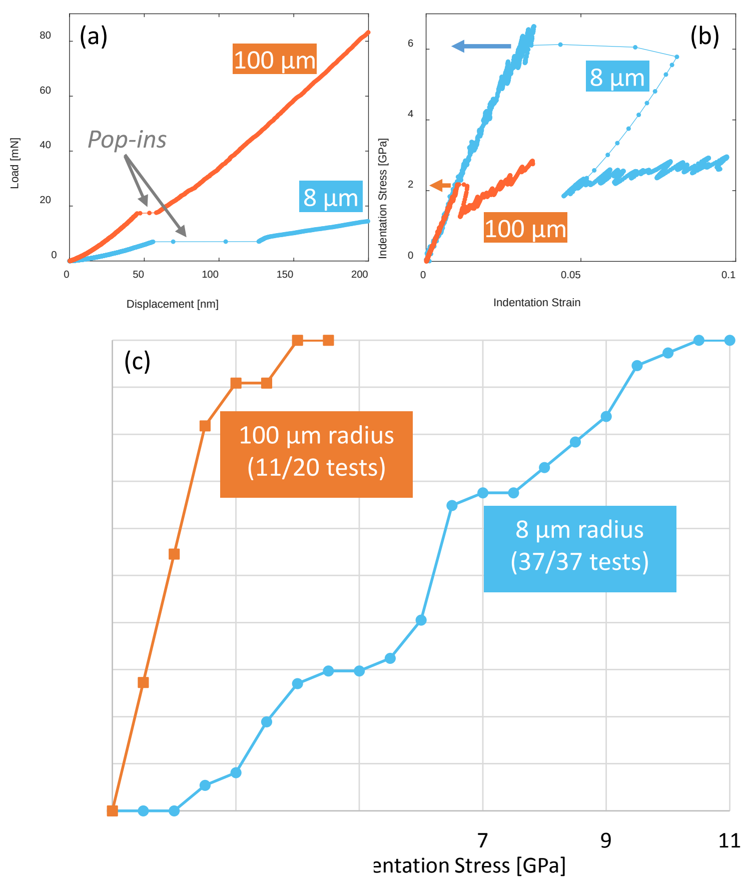


**Figure 7. (a) Representative load-displacement curves for the 8 and 100 micron radius indenters showing pop-ins (b) Representative indentation stress-strain curves for the 8 and 100 micron radius indenters showing the pop-in indentation stress. (c) Cumulative indentation pop-in stress distributions for both indenter sizes. The totals come from all test data across both alloys and zones (FZ and HAZ) in the welds. Note that roughly 50% of the 100 micron radius tests showed pop-ins while 100% of the 8 micron radius tests showed pop-ins.**

A comparison of the indentation stress-strain response between the FZ and HAZ for the 8 µm radius indenter on the two alloys is shown in Figure 8. The pop-in behavior and indentation stress following the pop-ins are similar in the FZ and HAZ. The HAZ has only marginally higher indentations stresses following the pop-in event. Similar grain orientations were tested to try to reduce grain orientation effects in the comparison. More tests are required to precisely determine the grain-scale anisotropy of the indentation stress-strain response on these alloys. The marginal differences between the FZ and HAZ are more evident in the 100 µm radius indentation stress-strain curves in Figure 9.

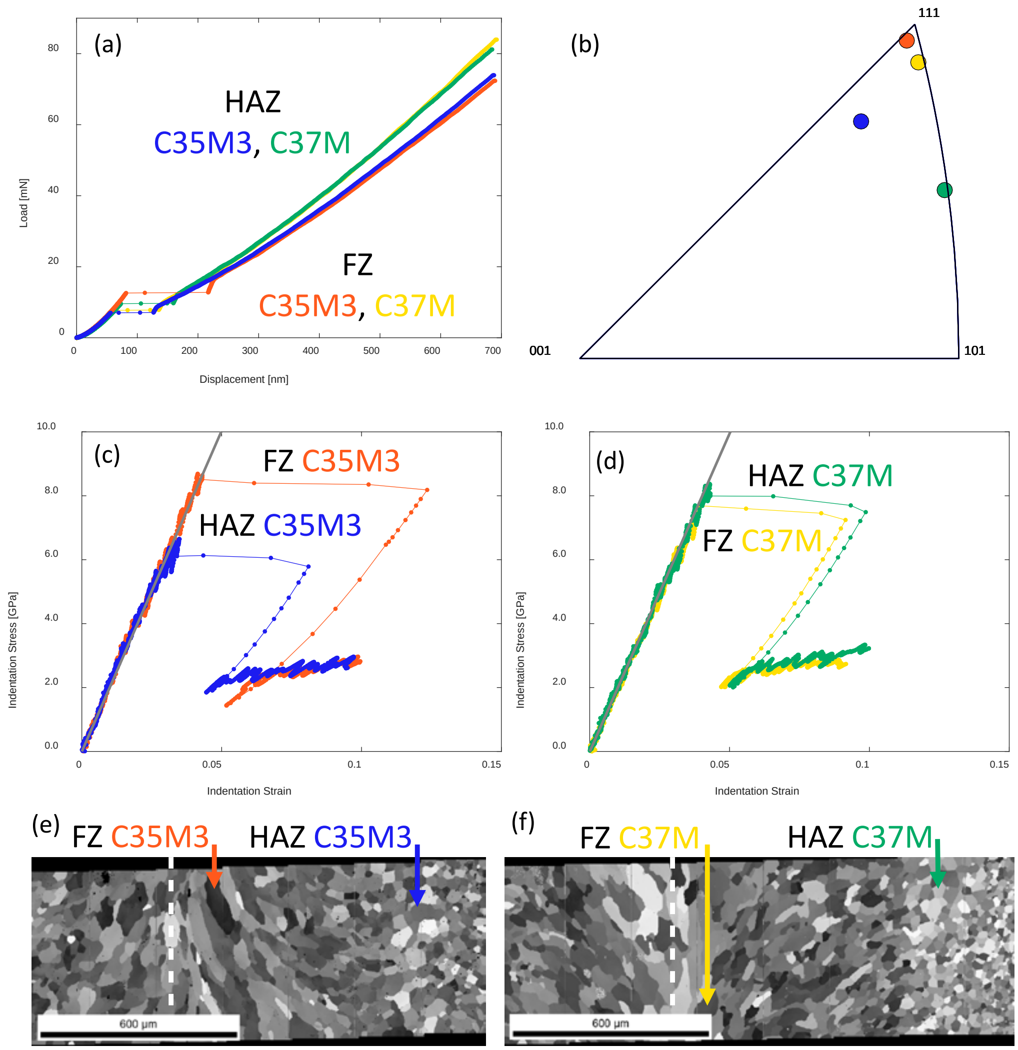


**Figure 8. (a) Representative load-displacement curves for 8 micron radius tests for C35M and C37M alloys in the FZ and HAZ, (b) corresponding grain orientations represented in the inverse pole figure, (c-d) indentation stress-strain curves, and (e-f) locations of tests on the weld microstructures (grayscale EBSD-IPF maps).**

The 100 µm radius indenter post-yield indentation stress for the HAZ in both alloys is consistently above the FZ tests as shown in Figure 9; however, it is also clear that they overlap so it is hard to argue that the difference is significant. Again the tests were done in similarly oriented grains to try to mitigate the differences between tests due to the grain orientation. Similar to the 8 µm radius indenter tests, there was no observable difference for the 100 µm radius indenter tests in terms of the pop-in behavior between the two alloys or two weld zones (FZ and HAZ).The average indentation properties for the two alloys is presented in Table 2 for the 100 µm radius indents. Since the difference between the FZ and HAZ was not significant, the average of both FZ+HAZ tests on the two alloys was calculated. It is clear that C37M has a higher average indentation yield strength, and both materials have similar average indentation moduli and work-hardening. Data on the AR samples is missing because it could not be reliably analyzed. This is likely a consequence of the small grain size and subsequent surface roughness due to lightly etched grain boundaries from electropolishing. Alternative sample preparation procedures are being explored such as vibratory polishing to produce a flatter surface comparable in quality to electropolishing.

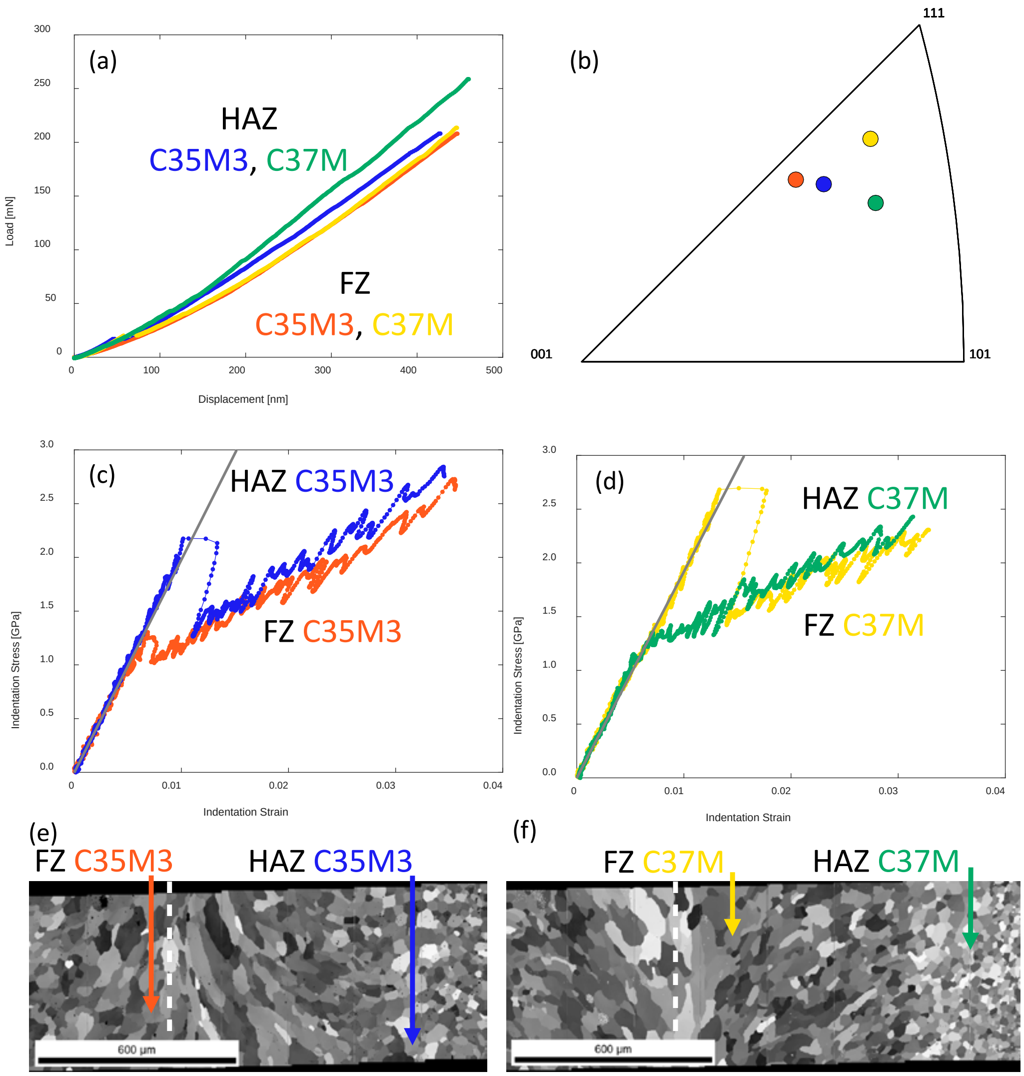


**Figure 9. (a) Representative load-displacement curves for 100 micron radius tests for C35M and C37M alloys in the FZ and HAZ, (b) corresponding grain orientations represented in the inverse pole figure, (c-d) indentation stress-strain curves, and (e-f) locations of tests on the weld microstructures (grayscale EBSD-IPF maps).**

**Table 2. Average indentation modulus, strength, and work-hardening values for C35M and C37M FeCrAl alloys in the FZ and HAZ. The error represents ± one standard deviation.**

| Sample | Indentation Modulus [GPa] | Indentation Strength [GPa] | Work-Hardening [GPa] | No. Tests |
|---|---|---|---|---|
| C35M FZ + HAZ | 196 ± 5 | 1.09 ± 0.08 | 50.9 ± 8.8 | 11 |
| C37M FZ + HAZ | 193 ± 8 | 1.32 ± 0.14 | 49.5 ± 6.5 | 9 |

# 4. Discussion

## 4.1 Weld-softening

It is notable that the grain-scale Berkovich nanohardness measurements on AR and welded material capture the same degree of weld-softening as tensile tests on polycrystalline samples for C35M and C37M FeCrAl alloys. C35M weld-softening was 16% for hardness and 18% for tensile yield strength measurements, and C37M weld-softening was 7% for hardness and 12% for tensile yield strength measurements. The differences between hardness and tensile yield strength weld-softening are within one standard deviation. This means that the change in grain size from the BM to the FZ is not a significant factor for the weld-softening (reduction in yield strength). Rather it is likely that changes at the grain-scale are the primary reason for weld-softening. It is believed that the change in the defect structure across the weld is the principal contribution to weld-softening. Note that deviations in chemical composition from the AR material were not investigated so this cannot not be ruled out as a contributing factor. However, it is clear from EBSD that AR C35M contains a moderate amount of deformed grains while C37M contains dramatically fewer deformed grains. We believe the FZ and HAZ in the welds are largely defect free, and thus have a nominally different defect structure from the BM. Within the weld, only recrystallized regions can be seen on EBSD maps, and spherical nanoindentation tests showed frequent pop-in events even for a 100 μm radius indenter which is characteristic of well-annealed metals (low defect densities). These changes in the defect structure (inferred from microstructure, indentation, and processing information) as a result of going from a moderately recrystallized microstructure to a completely recrystallized/annealed microstructure for C35M and a nearly fully recrystallized microstructure to a completely recrystallized/annealed microstructure are in good physical agreement with the difference in weld-softening between the two alloys. That is that C35M shows more weld-softening than C37M. In addition to useful correlations between hardness and tensile strength, nanoindentation tests offer additional insight into the microscale mechanical behavior of welded FeCrAl alloys and weld-softening behavior.

## 4.2 Spherical nanoindentation across gradient microstructures

The full potential of spherical nanoindentation testing was not realized since tests on the AR material were not completed. It is expected that additional tests on the BM or AR material will show differences in pop-in behavior, indentation strength, and possibly even indentation work-hardening. Tests on the AR material with the 100 μm indenter were not successful on electropolished samples. This is likely due to the fact that the indenter comes in contact with multiple grains/grain boundaries results in a relatively rough surface due to the nature of electropolishing which preferentially attacks grain boundaries. Thus a different sample preparation procedure such as vibratory polishing is required to produce a flatter surface at the length scale of the indentation contact area. Figure 10 shows the gradient in microstructure across the weld from the FZ to the BM and what can be probed with indenters with different radii. Ideally, we would measure single grains and/or a polycrystalline response using the same indenter size (to mitigate indenter size effects) across the entire microstructure. The grain boundary affected indents are not desirable for this study since the interpretation and analysis of the indentation stress-strain curve is more convoluted.

Making single grain measurements across the entire sample with the same indenter size would require a very small indenter radius due to the small grain size in the BM; however, the pop-ins in the FZ and HAZ would be even larger (larger stresses) due to nature of the pop-in indenter size effect. The reason this is undesirable is because the pop-in obscures the indentation yield point. Making polycrystalline measurements across the entire sample with the same indenter size would require using very large indenter radii in order to test volumes of material which contain multiple grains in the FZ (polycrystalline response). However, this is not feasible with current equipment due to the large load requirements

(>>10N). In addition, larger samples would be required. Rather there is likely some middle ground using a 100 µm radius indenter where we can test single grains in the FZ and HAZ and a polycrystalline response in the BM. The appropriate choice of the indenter size for characterizing gradient microstructures is critical for spherical indentation stress-strain measurements. One either has to accept and understand possible indenter size effects using different indenter sizes or accept and understand structural effects (single grain to polycrystalline) using a single indenter size in the comparison of the response across the microstructurally graded sample.

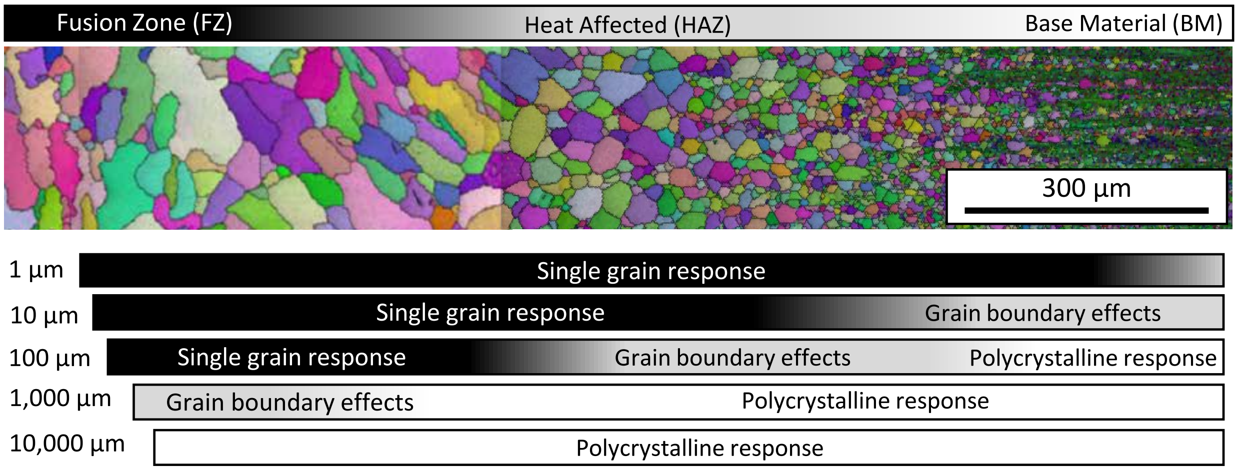


**Figure 10. Weld microstructure (modified from [5]) showing the FZ, HAZ, and BM. Listed below are the expected mechanical responses from different indenter sizes ranging from single grains/crystals to polycrystalline/bulk-like volumes. Note that only 10 (single grain) and 100 micron (single grain at the edge grain boundary effects) radius indenter measurements were made in the FZ and HAZ in this report.**

## 5. Conclusions

In this report we characterized the grain-scale response of the AR and welded material for FeCrAl alloys C35M and C37M using a combination of Berkovich and spherical tip nanoindentation. A comparison of the data generated from the two different techniques is shown in Figure 11. Berkovich nanohardness measurements showed weld-softening comparable to tensile yield strength measurements. This is strong evidence that the primary reason for weld-softening is due to changes in the grain-scale structure likely driven by changes in the defect structure between the AR and welded material. In addition, hardness measurements correlated well with tensile yield strength and UTS values. Spherical nanoindentation on the FZ and HAZ showed frequent pop-ins characteristic of a well annealed metal. Hardness and indentation yield strength measurements show that welded C37M has higher strength than welded C35M. Spherical nanoindentation tests also show that the alloys have similar work-hardening behavior. No modulus differences were observed for all nanoindentation experiments (C35M versus C37M and AR versus welded material). Indentation testing did not provide any indication that welded C37M would behave more brittle than the AR material. This behavior likely can only be observed with tensile or fracture testing.

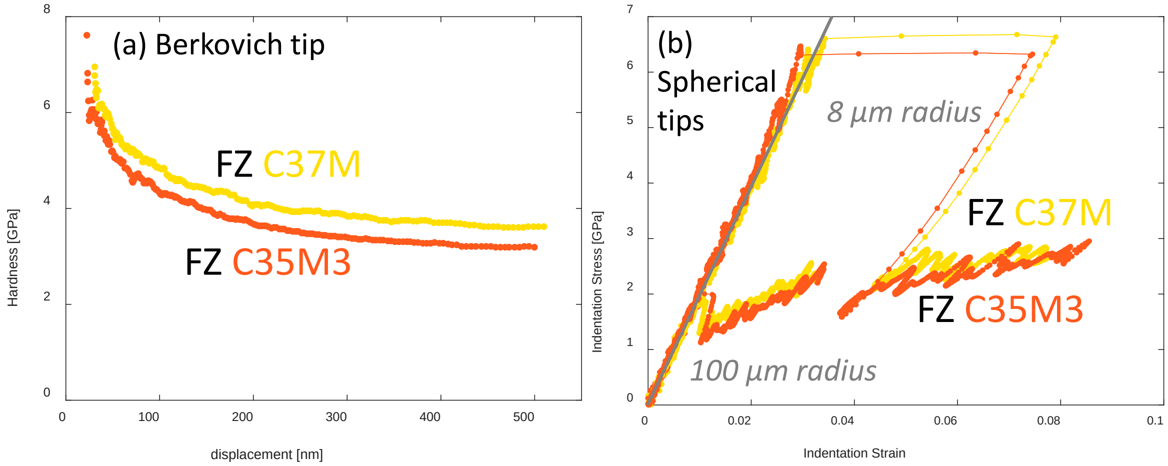


**Figure 11. Comparison of indentation measurements from pyramidal and spherical tip protocols. (a) Representative Berkovich hardness versus indentation depth in the FZ for C35M and C37M alloys (see Table 1 for quantitative results). (b) Representative indentation stress-strain curves for spherical tips in the FZ for C35M and C37M (see Table 2 for quantitative results). Note all tests shown are inside individual grains.**

## 6. Future Work

There are several future tasks focused on additional indentation testing of the AR and welded material followed by irradiation experiments and indentation testing.

- Establish a polishing procedure that produces less relief at grain boundaries, and characterize the BM of C35M and C37M with spherical nanoindentation.
- Try to correlate the spherical nanoindentation stress-strain response with regions of un-recrystallized and recrystallized grains on the BM.
- Correlate the indentation stress-strain response with crystal orientation for single grain measurements in the FZ in order to quantify the grain-scale anisotropy of these FeCrAl alloys.
- Ion irradiate BM and weld samples followed by indentation testing to quantify radiation hardening.

## 7. References

[1] R.B. Rebak, K.A. Terrani, W.P. Gassmann, J.B. Williams, K.L. Ledford. Improving Nuclear Power Plant Safety with FeCrAl Alloy Fuel Cladding, MRS Advances (2017) 1-8.

[2] Y. Yamamoto, B.A. Pint, K.A. Terrani, K.G. Field, Y. Yang, L.L. Snead. Development and property evaluation of nuclear grade wrought FeCrAl fuel cladding for light water reactors, J Nucl Mater 467, Part 2 (2015) 703-716.

[3] K.G. Field, M.N. Gussev, Y. Yamamoto, L.L. Snead. Deformation behavior of laser welds in high temperature oxidation resistant Fe–Cr–Al alloys for fuel cladding applications, J Nucl Mater 454 (2014) 352-358.

[4] S.J. Zinkle, K.A. Terrani, L.L. Snead. Motivation for utilizing new high-performance advanced materials in nuclear energy systems, Current Opinion in Solid State and Materials Science 20 (2016) 401-410.

[5] K.G. Field, M.N. Gussev, Y. Yukinori, R. Howard, S. Briggs. Second Annual Progress Report on Radiation Tolerance of Controlled Fusion Welds in High Temperature Oxidation Resistant FeCrAl Alloys. Oak Ridge National Laboratory, 2016.
[6] M.N. Gussev, K.G. Field, Y. Yamamoto. The analysis of the general performance and mechanical behavior of unirradiated FeCrAl alloys before and after welding. Oak Ridge, TN: Oak Ridge National Laboratory, 2016.
[7] P. Hosemann, C. Vieh, R.R. Greco, S. Kabra, J.A. Valdez, M.J. Cappiello, S.A. Maloy. Nanoindentation on ion irradiated steels, J Nucl Mater 389 (2009) 239-247.
[8] V.H. Baltazar Hernandez, S.K. Panda, M.L. Kuntz, Y. Zhou. Nanoindentation and microstructure analysis of resistance spot welded dual phase steel, Mater Lett 64 (2010) 207-210.
[9] O. Anderoglu, E. Aydogan, S.A. Maloy, Y. Wang. Ion Irradiation Testing and Characterization of FeCrAl Candidate Alloys. Los Alamos, NM: Los Alamos National Laboratory, 2014.
[10] S.R. Kalidindi, S. Pathak. Determination of the effective zero-point and the extraction of spherical nanoindentation stress-strain curves, Acta Materialia 56 (2008) 3523-3532.
[11] J.S. Weaver, S. Pathak, A. Reichardt, H. Vo, S.A. Maloy, P. Hosemann, N. Mara. Spherical nanoindentation of proton irradiated 304 stainless steel: a comparison of small scale mechanical test techniques for measuring irradiation hardening, J Nucl Mater (submitted).
[12] J.S. Weaver, A. Khosravani, A. Castillo, S.R. Kalidindi. High throughput exploration of process-property linkages in Al-6061 using instrumented spherical microindentation and microstructurally graded samples, Integrating Materials and Manufacturing Innovation 5 (2016) 1-20.
[13] D.K. Patel, S.R. Kalidindi. Correlation of spherical nanoindentation stress-strain curves to simple compression stress-strain curves for elastic-plastic isotropic materials using finite element models, Acta Materialia 112 (2016) 295-302.
[14] J. Hay, P. Agee, E. Herbert. Continuous Stiffness Measurement During Instrumented Indentation Testing, Experimental Techniques 34 (2010) 86-94.
[15] X.D. Li, B. Bhushan. A review of nanoindentation continuous stiffness measurement technique and its applications, Materials Characterization 48 (2002) 11-36.
[16] W.C. Oliver, G.M. Pharr. Measurement of hardness and elastic modulus by instrumented indentation: Advances in understanding and refinements to methodology, J Mater Res 19 (2004) 3-20.
[17] S. Pathak, S.R. Kalidindi. Spherical nanoindentation stress-strain curves, Mat Sci Eng R 91 (2015) 1-36.
[18] J.J. Vlassak, W.D. Nix. Measuring the elastic properties of anisotropic materials by means of indentation experiments, Journal of the Mechanics and Physics of Solids 42 (1994) 1223-1245.
[19] D.K. Patel, H.F. Al-Harbi, S.R. Kalidindi. Extracting single-crystal elastic constants from polycrystalline samples using spherical nanoindentation and orientation measurements, Acta Materialia 79 (2014) 108-116.
[20] H. Hertz, D.E. Jones, G.A. Schott. Miscellaneous papers, Macmillan and co., London, New York, 1896.
[21] K.L. Johnson. Contact mechanics, Cambridge University Press, Cambridge Cambridgeshire ; New York, 1985.
[22] Y. Huang, F. Zhang, K.C. Hwang, W.D. Nix, G.M. Pharr, G. Feng. A model of size effects in nano-indentation, Journal of the Mechanics and Physics of Solids 54 (2006) 1668-1686.
[23] J.G. Swadener, E.P. George, G.M. Pharr. The correlation of the indentation size effect measured with indenters of various shapes, Journal of the Mechanics and Physics of Solids 50 (2002) 681-694.
[24] W.D. Nix, H.J. Gao. Indentation size effects in crystalline materials: A law for strain gradient plasticity, Journal of the Mechanics and Physics of Solids 46 (1998) 411-425.
[25] G.M. Pharr, E.G. Herbert, Y.F. Gao. The Indentation Size Effect: A Critical Examination of Experimental Observations and Mechanistic Interpretations, Annu Rev Mater Res 40 (2010) 271-292.
[26] Z.T. Thompson, K.A. Terrani, Y. Yamamoto. Elastic Modulus Measurements of ORNL ATF FeCrAl Alloys. Oak Ridge, TN: Oak Ridge National Laboratory, 2015.

[27] A. Bolshakov, G. Pharr. Influences of pileup on the measurement of mechanical properties by load and depth sensing indentation techniques, J Mater Res 13 (1998) 1049-1058.
[28] D. Tabor. The hardness of metals, Clarendon Press, Oxford,, 1951.
[29] A. Lupinacci, K. Chen, Y. Li, M. Kunz, Z. Jiao, G.S. Was, M.D. Abad, A.M. Minor, P. Hosemann. Characterization of ion beam irradiated 304 stainless steel utilizing nanoindentation and Laue microdiffraction, J Nucl Mater 458 (2015) 70-76.
[30] H.R. Higgy, F.H. Hammad. Effect of fast-neutron irradiation on mechanical properties of stainless steels: AISI types 304, 316 and 347, J Nucl Mater 55 (1975) 177-186.
[31] B.R. Donohue, A. Ambrus, S.R. Kalidindi. Critical evaluation of the indentation data analyses methods for the extraction of isotropic uniaxial mechanical properties using finite element models, Acta Materialia 60 (2012) 3943-3952.
[32] S. Pathak, J.L. Riesterer, S.R. Kalidindi, J. Michler. Understanding pop-ins in spherical nanoindentation, Appl Phys Lett 105 (2014).
[33] P.S. Phani, K.E. Johanns, E.P. George, G.M. Pharr. A stochastic model for the size dependence of spherical indentation pop-in, J Mater Res 28 (2013) 2728-2739.
[34] S. Shim, H. Bei, E.P. George, G.M. Pharr. A different type of indentation size effect, Scripta Materialia 59 (2008) 1095-1098.
[35] S.R. Kalidindi, S. Pathak, D. Stojakovic. Measurement of the local mechanical properties in polycrystalline samples using spherical nanoindentation and orientation imaging microscopy, Acta Materialia 57 (2009) 3020-3028.
[36] S.J. Vachhani, S.R. Kalidindi. Grain-scale measurement of slip resistances in aluminum polycrystals using spherical nanoindentation, Acta Materialia 90 (2015) 27-36.
[37] S. Pathak, D. Stojakovic, R. Doherty, S.R. Kalidindi. Importance of surface preparation on the nano-indentation stress-strain curves measured in metals, J Mater Res 24 (2009) 1142-1155.
[38] S. Pathak, D. Stojakovic, S.R. Kalidindi. Measurement of the local mechanical properties in polycrystalline samples using spherical nanoindentation and orientation imaging microscopy, Acta Materialia 57 (2009) 3020-3028.